Sensors and Actuators B 249 (2017) 14–21

Contents lists available at ScienceDirect

Sensors and Actuators B: Chemical

journal homepage: www.elsevier.com/locate/snb

# LSPR sensor array based on molecularly imprinted sol-gels for pattern recognition of volatile organic acids

Liang Shang[a], Chuanjun Liu[a,b], Masashi Watanabe[a], Bin Chen[c], Kenshi Hayashi[a,*]

[a] Department of Electronics, Graduate School of Information Science and Electrical Engineering, Kyushu University, Fukuoka 819-0395, Japan
[b] Research Laboratory, U.S.E. Co., Ltd., Tokyo 150-0013, Japan
[c] College of Electronic and Information Engineering, Southwest University, Chongqing 400715, China

ARTICLE INFO

*Article history:*
Received 14 October 2016
Received in revised form 5 April 2017
Accepted 8 April 2017
Available online 14 April 2017

*Keywords:*
Human body odor
Volatile organic acid
Localized surface plasma resonance
Molecularly imprinted sol-gel
Sensor array
Linear discriminant analysis

ABSTRACT

Volatile organic acids are important compounds contained in human body odor. The detection and recognition of volatile organic acids in human body odor are significant in many areas. The present study explored a possibility to use localized surface plasmon resonance (LSPR) of Au nanoparticles (AuNPs) and molecularly imprinted sol-gels (MISGs) as the sensitive layer to recognize typical organic acid odorants, propanoic acid (PA), hexanoic acid (HA), heptanoic acid (HPA) and octanoic acid (OA), from human body. The LSPR layer was prepared by vacuum sputtering of AuNPs on a glass substrate and consequently thermal annealing. The sensitive layer was fabricated by spin-coating molecularly imprinted titanate sol-gel on the AuNPs layer. A homemade optical device was developed to detect the change of transmittance, which was caused by the index changes of organic acid vapors where selecting absorbed by the MISG layers. It was found that compared with MISG coated samples, samples coated with non-imprinted sol gel (NISG) shown no responses to any acid vapors. For the MISG coated sensors, the LSPR sensitivity was affected by the spin coating speed. In addition, a sensor array based on MISGs with different templates (HA, HPA and OA) was constructed to detect the organic acids in single and their binary mixtures. The sensor response was analyzed by principal component analysis (PCA) and linear discriminant analysis (LDA). A 100% classification rate was achieved by leave-one-out cross-validation technique for LDA model. This work demonstrated that the MISGs coated LSPR sensor array has a great potential in organic acid odor recognition of human body odor.



## 1. Introduction

Human body odors emitted from skin and body parts are caused by gender, age, heredity, physiological condition and food habits etc. [1,2]. Based on those odors alone, people can assess various personal features of others accurately [3]. Hence, human body odor would be applied in medical diagnosis and forensic expertise [4,5]. It has been demonstrated that human body odor is comprised by diverse VOCs, such as low molecular weight fatty acids, aldehydes, ketones, amines, alcohols, esters, etc. [6–8]. Among these odorants, organic acids ($C_5$–$C_{11}$) are considered as typical odorants from difference human body parts, such as foot odor and underarm odor [9]. Traditionally, human body odor has been analyzed by gas chromatography/mass spectrometer (GC/MS) method [10,11]. However, GC/MS is not suitable for on-line detection because of its high-cost, time-consuming and bulky size etc. [12]. Therefore, novel sensors need to be explored for detecting organic acid from human body odor. Recently, some sensors, such as microbial fuel cell (MFC) sensors, optical fiber sensors, fluorescent imaging sensors and quartz crystal microbalance (QCM) sensors, are successfully developed for organic acid detection [6,9,13–15].

The phenomenon of localized surface plasmon resonance (LSPR), which results from the plasmonic response of nanoparticles by incident electromagnetic waves, can be applied in sensing of analytes [16–21]. The mechanism is based on detecting the change of environmental refractive index (RI) [20–22]. Compared with other transducers, such as metal oxide semiconductor (MOS) sensors and QCM sensors, the superiorities of LSPR sensors are high-speed response and rapid recovery, which had been proved by our previous to be suitable in gas and odor sensing [17].

However, the single LSPR sensors are non-specificity sensors. To solve this problem, molecularly imprinted polymer (MIP) was employed as the sensitive layer to realize the selectivity for LSPR

* Corresponding author.
*E-mail addresses:* shang.liang.100@s.kyushu-u.ac.jp (L. Shang), liu@o.ed.kyushu-u.ac.jp (C. Liu), watanabe@o.ed.kyushu-u.ac.jp (M. Watanabe), chenbin121@swu.edu.cn (B. Chen), hayashi@ed.kyushu-u.ac.jp (K. Hayashi).

http://dx.doi.org/10.1016/j.snb.2017.04.048
0925-4005/

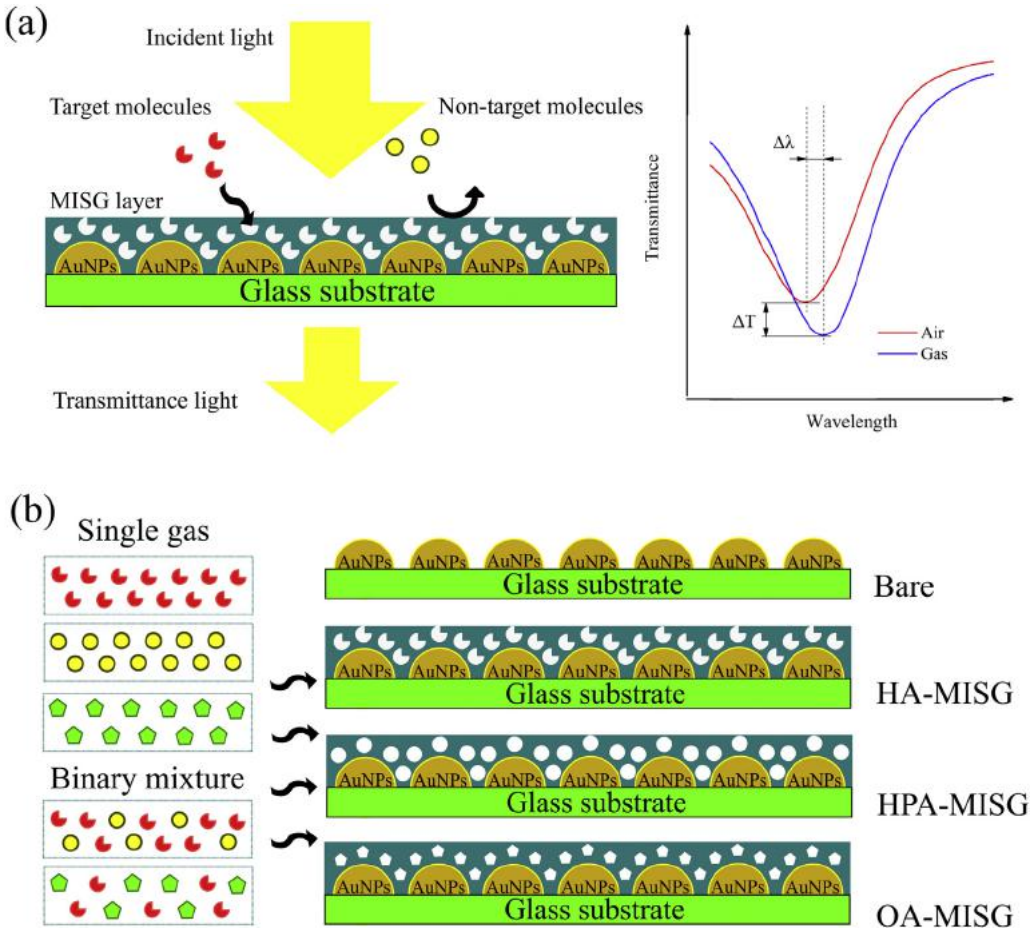


**Fig. 1.** The schematic graph of MISG-coated AuNPs film for selective organic acid detection (a) and MISG-LSPR multichannel sensor platform for organic acid vapors mixture detection (b).

sensors [23]. Molecular imprinting is an effective approach for creating recognition patterns of diverse length scales for molecules [24–26]. By adding templates in the starting material, recognition sites would be generated in these polymer materials [27]. When the templates were removed from the polymer matrix by washing or heating, nano-scale cavities similar to the template molecules were generated [28]. Through these high specificity cavities, MIP had been applied as a highly selective sensitive layer to some transducers, such as QCM sensors [29–32]. Our previous work has demonstrated that the introduction of MIP as a sensitive layer is an effective approach to increase the selectivity of LSPR sensor, which has been used in the selective detection of terpene vapors [33–35]. Different from polymers, sol-gel materials are competitive in the stability of chemical and thermal [27]. Therefore, sol-gel material would be more suitable in developing optical sensors for gas detection.

In present work, MISG was employed as the special adsorption layer for LSPR sensors. The schematic diagram of MISG coated LSPR sensor is shown in Fig. 1a. Based on the unusual cavities generated in sol-gel matrix, the target organic acid vapor would be absorbed selectively. And it would induce the change of surface plasmon peak position ($\lambda_{min}$) and the transmittance variation in spectrum. By detecting these variations, an optical sensor for organic acid vapors detection would be developed. In addition, human body odor is always composed by diverse of organic acid vapors [3]. Hence, to detect the mixture of organic acid vapors is another topic in body human odor determination. Here, three MISG films generated by different organic acid templates, hexanoic acid (HA), heptanoie acid (HPA) and octanoic acid (OA), were coated on Au nano-island layers for establishing a MISG-LSPR multichannel sensor platform (Fig. 1b). The response matrix was obtained by measuring for organic acid vapors: propanoic acid (PA), HA, HPA and OA, in single and their binary mixtures. Finally, the response matrix was processed and analyzed by principal component analysis (PCA) and linear discriminant analysis (LDA) for odor pattern recognition. The feasibility of the developed MISG-LSPR sensor array for determination of organic acid vapors was discussed and evaluated.

## 2. Material and methods

### 2.1. Chemicals and reagents

Tetrabutoxy titanium (TBOT), *iso*-propanol, PA, HA, HPA, OA, titanium tetrachloride ($TiCl_4$), acetone and ethanol were purchased from Wako Pure Chemical Industries, Japan. 3-aminopropyl triethoxysilane (APTES) was purchased from Shin-Etsu Chemical, Japan. All of the reagents were used as received.

### 2.2. Synthesis of MISG reaction solutions

MISGs reaction solution was prepared by dissolving 136 μL TBOT as a precursor, 50 μL of template molecules and 24 μL APTES as a functional monomer in 2 mL of *iso*-propanol. Here, HA, HPA and OA were selected as the template molecules. Afterwards, 25 μL

$TiCl_4$ was added to initialize the reaction. Finally, the reaction solution was prehydrolyzed in a 70 °C water bath for 1 h.

### 2.3. MISG coated Au nano-island film preparation

Concisely, a TIO glass substrate was cleaned by ultrapure water, acetone and ethanol and dried with nitrogen flow, successively. After argon plasma cleaned for 5 min (PDC-001, Harrick plasma, USA), the substrate was immersed in a 1:10 (v:v) ethanol solution of APTES for 8 h. The substrate was cleaned with ethanol and drying with nitrogen flow, and put into a quick coater (SC-701 HMCII, Sanyu electron, Japan) for AuNPs deposition, the thickness was set as 3 nm by tuning the deposition current. Then, the sample was annealed in air atmosphere at 200 °C for 5 h in a muffle furnace (SSTS-13 K, ISUZU, Seisakusho, Japan) and cooled naturally till room temperature (25 °C). Afterwards, MISG layers were coated on the AuNPs film by spin coating 20 μL of its reaction solution. As the last step, the sample was heated at 200 °C for 1 h for constructing the MISG layer and removing the template molecules.

### 2.4. Vapor generating system

The vapor generating system used in this study is shown in Fig. 2a. It was consisted of an air pump (LV-125A, Linicon, Japan), an air-cleaning filter filled with molecular sieves and activated carbon, 2 mass flow controllers (MFC) (3660, Kofloc, Japan), a 3 way solenoid valve (FSM-0408Y, FLON Industry, Japan), a glass bottle (6 mL) and a personal computer. Pure dry air was as the diluting gas in this study. All the gas flow paths were connected by Teflon tubes. Through a NI DAQ (USB-6009, National instruments, Austin, USA) card and LabView software (National instruments, Austin, USA), two MFCs and the gas valve can be controlled by the personal computer. The concentration $C$ (ppm) of single organic acid vapor can be calculated by Eq. (1).

$$C = \frac{k \times D_r \times 10^3}{F} \quad (1)$$

where $D_r$ (μg/min) indicted the diffusion rate at the appoint temperature, $F$ (L/min) indicated the flow rate of diluent gas, $k$ indicated the factor for converting gas weight to gas volume, which can be calculated as follows:

$$k = \frac{22.4 \times (273 + t) \times 760}{M \times 273 \times P} \quad (2)$$

where $M$ indicated the molecular weight of organic acid molecule, $t$ is the gas temperature and $P$ is the gas pressure (760 mmHg). In this work, single organic acid vapor was generated by injecting 2 mL of each of organic acids (PA, HA, HPA or OA) in the glass bottle. Binary mixture of acid vapors (A + B) was generated by injecting 1 mL of organic acid A and 1 mL of organic acid B in the glass bottle together. In this study, 3 types of binary mixtures (PA + HA, PA + OA, HA + OA) were considered. Cleaned glass bottles were used for each testing. The flow rates of diluent air were set as 0.6, 0.5 and 0.4 L/min, respectively.

### 2.5. Organic acid vapor sensing system

SEM (SU8000, Hitachi, Japan) was employed to analyze the morphology characteristics of Au nano-islands before and after sol-gel deposition in this study. The schematic of transmittance spectra measurement system is show in Fig. 2b. The system was included a light source (LS-1 tungsten halogen light source, Ocean optics, USA), a UV spectrometer (HR4000, Ocean optics, USA), a homemade sensing cell (Teflon), 2 optical fibers (Ocean optics, USA) and a personal computer. By the software named OPwave+ (Ocean optics, USA), the transmittance spectra in real-time were detected and recorded. The scanning range was set from 400 to 900 nm, and the wavelength resolution was 0.1 nm. The actual photo for the experimental system and MISG-LSPR electrode in sensing cell was provided in Fig. 2c.

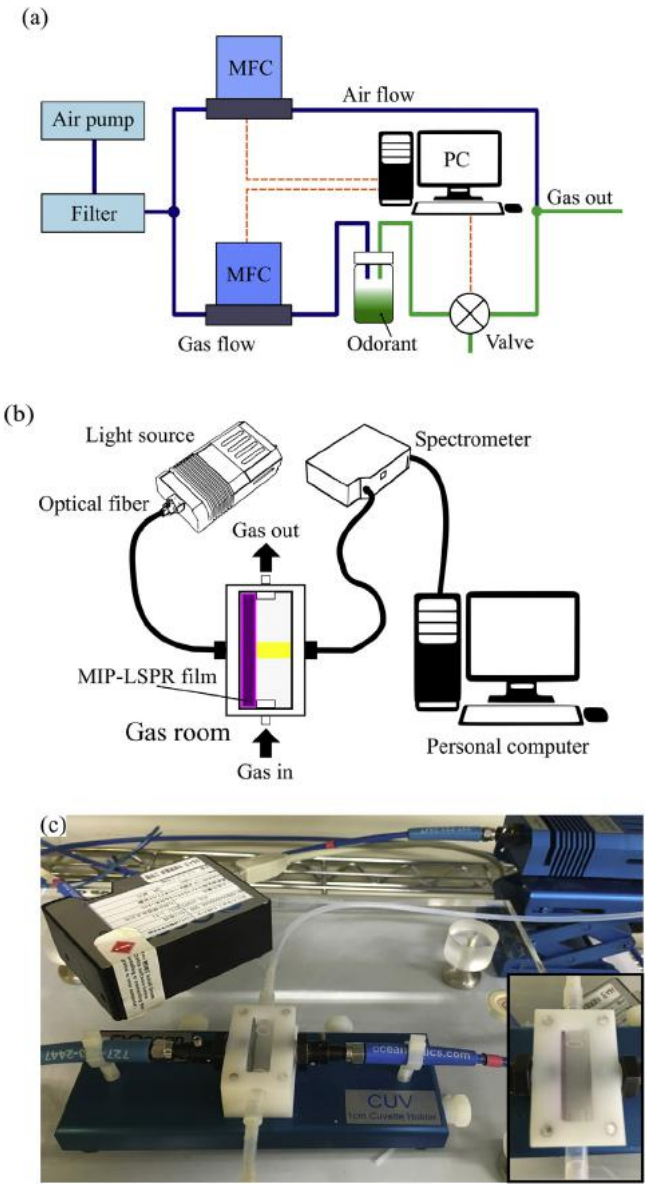


**Fig. 2.** Schematics of vapor generation system (a) and sensing system (b). The photo of the experimental system (c) and the MISG-LSPR electrode in the sensing cell.

## 3. Results and discussion

### 3.1. UV-vis spectra and vapor absorption characteristics of MISG coated AuNPs film

The thickness of MISG layer is a critical factor to its selective absorbability and it can be controlled by spin coating speed [34]. Firstly, the influence of the spin coating speed on optical characteristics of MISG/NISG coated Au nano-island films were investigated. The transmission spectra of bare, NISG and HA-MISG coated Au nano-island versus different spin coating speeds (1000 rpm, 3000 rpm and 5000 rpm) were shown in Fig. 3a. It was demonstrated that the sol-gel layer makes the plasmon peak shift to the red and the transmittance decrease (Fig. 3b). Besides, with the increase in spin coating speed, the transmittance was increased.

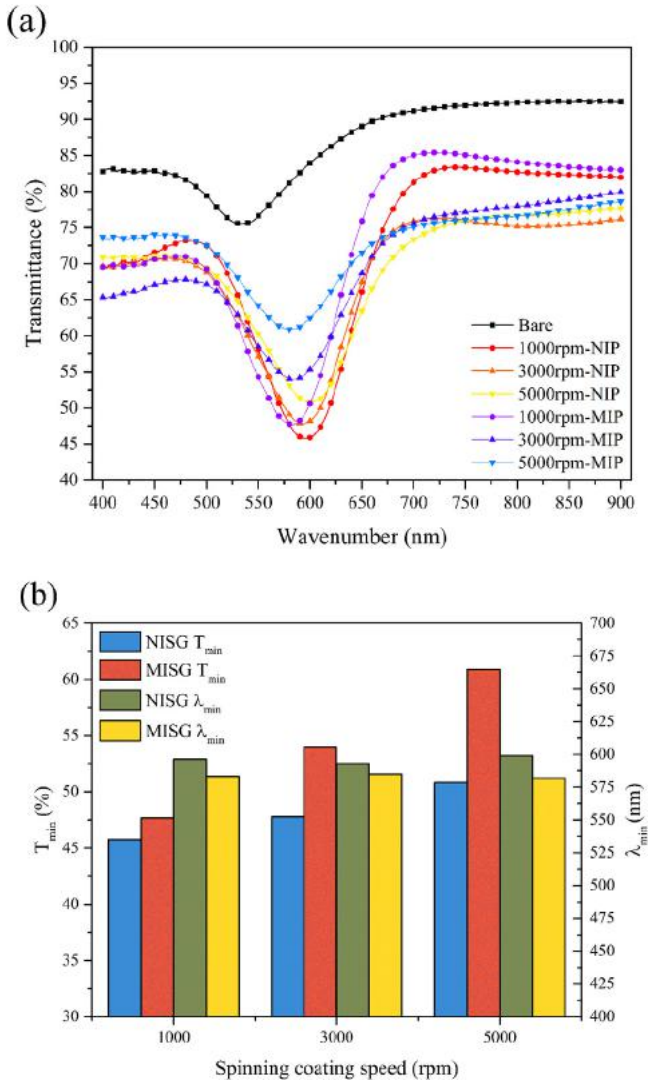


**Fig. 3.** Transmittance spectra (a) and optical features ($\lambda_{min}$ and $T_{min}$) (b) of NISG and HA-MISG coated AuNPs versus different spin coating speeds.

In addition, the minimum transmittances of samples coated with NISG were lower than those coated with MISG at the same spin coating speed. These transmittance decrease and spectral position red shift showed a spin coating speed dependent feature.

To determine the optimal coating speed for MISG layers, the real-time response characters of Bare/NISG/HAMISG coated sensors to HA vapor were investigated. The changes of transmittance at plasmon peak ($\lambda_{min}$) were detected and recorded. The $\Delta T$ can be calculated by formula as follows.

$$\Delta T = T - T_0 \tag{3}$$

where $T_0$ indicated the transmittance in air, and $T$ indicated the transmittance in organic acid vapors. The real-time response to HA vapor was as shown in Fig. 4. To investigate the changes of LSPR response before and after coated MISG/NISG layers, bare Au nano-island was also considered in this study. The RIS of surface plasmon (SP) extinction bands to dielectric properties of the surrounding medium was depended on the particle size and the distance between particles [23]. The surface morphology of bare Au nano-island was studied as shown in Fig. 5a. It indicated that all AuNPs were formed as arrays, which would induce a stranger RIS for LSPR [36].

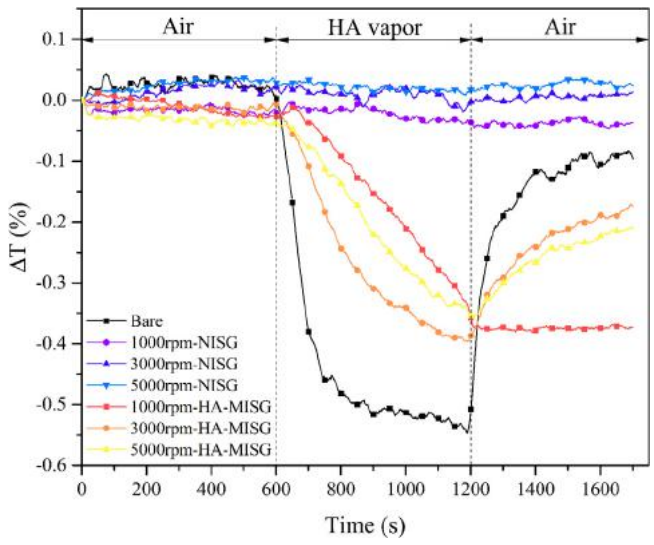


**Fig. 4.** Real-time response of HA-MISG and NISG with different coating speeds to HA vapor. Gas responses were obtained by keeping the switch on to HA vapor flow for 600 s and then to air flow for 600 s.

Fig. 4 showed that the response of bare sample was larger, and its response time was faster than NISG or MISG coated samples. Compared with MISG/NISG coated samples, more HA molecules could be absorbed in the RI sensing volume (SV) of AuNPs, and it would induce a stranger response for the vapor. We can also find that no responses were observed on samples coated NISG. It indicated that the adsorption capacity of pure titanate sol-gel matrix was weak, which agree with the results reported by Matsuguchi et al. [27]. The SEM image for NISG coated sample (spin coating speed 3000 rpm) is shown in Fig. 5b. It suggested that the surface of NISG was full of cracks. Compared with MISG coated samples (Fig. 5c), NISG coated sample showed a relative smooth surface and its surface area was smaller. This surface morphology would induce its poor gas responses. Besides, gas molecules would be obstructed by the pure sol-gel layer to be in the SV of AuNPs. Compared with the bare sample, the responses of MISG coated samples were smaller. It could be explained that only the molecules absorbed by the nanoscale cavities of MISG in SV could be sensed. By the effect of MISG layer, a longer response and recovery time was observed in in-situ responses. Besides, too thick layer (spin coating speed: 1000 rpm) would induce a longer recovery time. Just like we discussed in former work, excessive thin MIP layer is difficult to realize a good selectivity for target molecules, while thick layer would induce a long recovery time [34]. Considered the response and recovery time simultaneously, the relative optimal spin coating speed was selected as 3000 rpm in this study.

To determine the absorption characteristics of HA-MISG films to HA vapor, the in-situ responses of HA-MISG coated LSPR sensor (spin coating speed: 3000 rpm) to PA, HA and OA vapors were investigated. The normalized response $K$ can be defined by function 4.

$$K_j = \Delta T / C_j \tag{4}$$

where $j$ is on behalf of 3 types of organic acid vapors: PA, HA and OA. $C_j$ is the concentration of organic acids. Here, the concentrations of PA, HA and OA were 40.93, 21.05 and 11.23 ppm, respectively. Fig. 6 shows that the corresponding response signal of HA (0.01844) is the larger than that for PA (0.00523) or OA (0.00781). A faster response speed was also observed to HA vapor. Besides, the recovery time for HA is longer than other vapors. It indicated that more target gas molecules were absorbed in the SV of AuNPs, which would be contributed by the selectivity of the MISG layer.

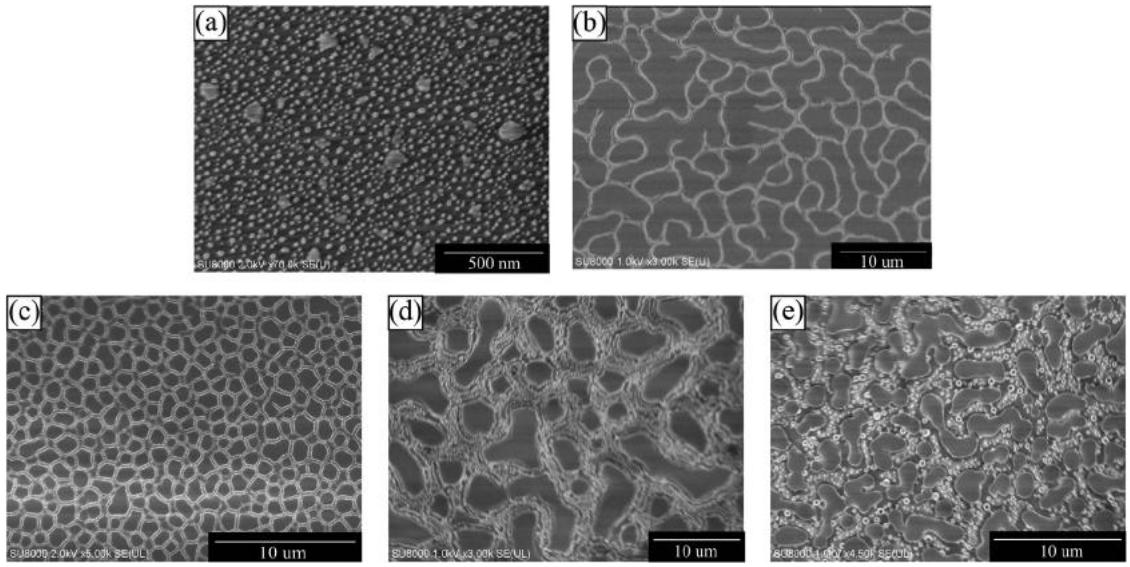


**Fig. 5.** SEM images of bare Au nano-island (a) and coated with NISG (b), HA-MISG (c), HPA-MISG (d) and OA-MISG (e). All the MISG/NISG films were fabricated by spin coating speed at 3000 rpm.

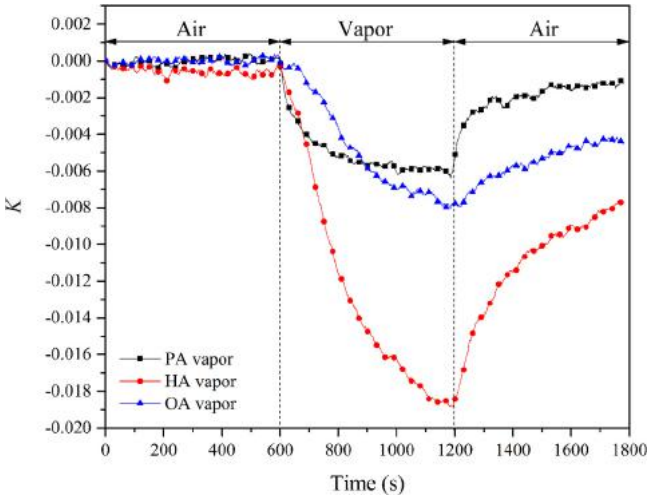


**Fig. 6.** Real-time responses of HAMISG-LSPR sensor to three fatty acid vapors (PA/HA/OA). Gas responses were obtained by keeping the switch on to organic acid vapor flow for 600 s and then to air flow for 600 s. The concentrations of PA, HA and OA were 40.93, 21.05 and 11.23 ppm. The $K_{min}$ for PA, HA and OA were −0.00523, −0.01844 and −0.00781, respectively.

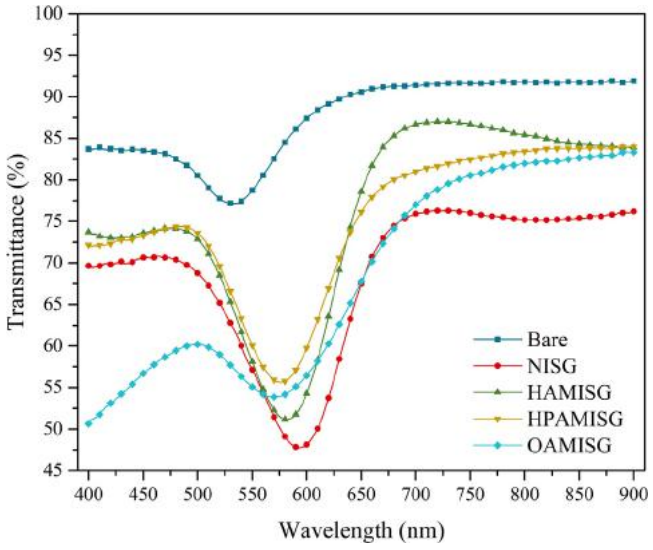


**Fig. 7.** Transmittance spectra of bare, NISG and three types of MISGs (HA-MISG/HPA-MISG/OA-MISG) coated samples.

### 3.2. Sensor array response for organic acid odors

By spin coating 3 types of MISG reaction solutions at 3000 rpm on Au nano-island layers, a MISG-LSPR sensor array was constructed. The sensor array was consisted of 4 channels: bare, HA-MISG, HPA-MISG and OA-MISG (Fig. 1b). The transmission spectra for 3 types of MISG coated samples were shown in Fig. 7. It suggested that by spin coating different type of MISGs, their $\lambda_{min}$ and $T_{min}$ were different. SEM images for different types of MISG coated samples are shown in Fig. 5. It illustrated that AuNPs were covered by MISG films. We can also find that the surfaces of MISG coated samples were full of cracks, and the degrees of tearing and roughnesses were different. Therefore, the surface areas of MISG coated sample are larger than NISG coated samples', which would induce the different response intensities. By adding template molecules, the polymerization of sol-gel can be effected, which would be explained these diverse morphologies. Because the size of cavities generated by template molecules in MISG films were too small, it is different to observe from SEM images.

For each measurement, sensors were exposed in dry air for 300 s firstly. Then, the target vapor exposure time 60 s and dry air was passed for next 300 s for recovery. By changing the flow rates (0.4 L/min, 0.5 L/min and 0.6 L/min), 3 concentrations of a vapor would be obtained. A typical response of HA-MISG coated LSPR sensor to 4 types of organic acid vapor (flow rate: 0.5 L/min) was shown in Fig. 8. In this study, 9 samples (3 concentrations × 3 repetitions) from 7 types of vapors (PA, HA, HPA, OA, PA + HA, PA + OA, HA + OA), total 63 samples were considered. Hence, a response ($\Delta T$) matrix $M_{63\times4}$ for the sensor platform could be obtained for subsequent research.

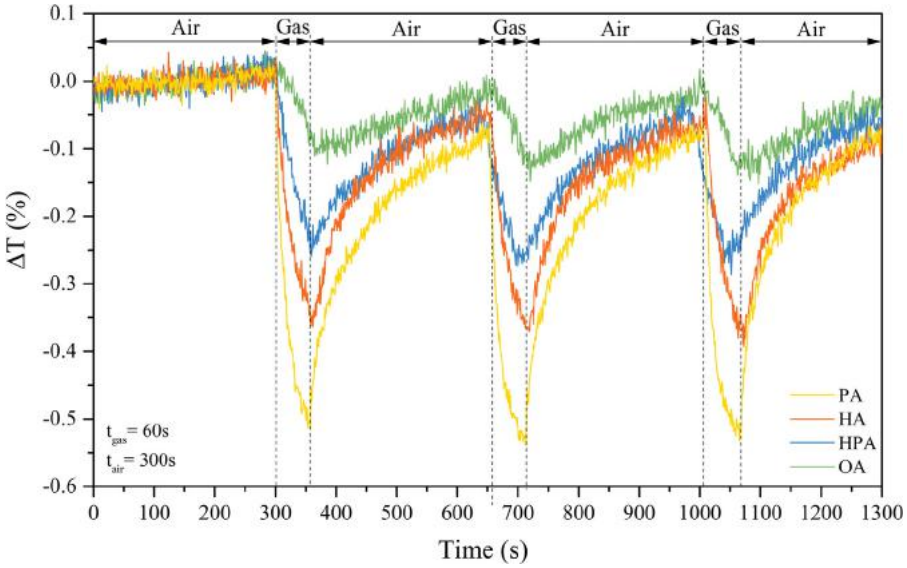


**Fig. 8.** Typical response of HA-MISG coated LSPR sensor to fatty acid vapors. Gas responses were obtained by keeping the switch on to organic acid vapor flow for 60 s and then to air flow for 300 s.

### *3.3. Discrimination of single or binary mixture of organic acid vapors*

Before discriminating, the matrix was pre-processed by autoscaling to reduce the large variations in response data for different channels. To visualize the cluster trends of vapor samples, PCA was performed on the normalized response matrix. PCA is a conventional unsupervised linear method for information concentrating, noise removing and data visualization [37]. By this method, principal components (PC) could be constructed by linear combination of the original variables [38]. Based on these uncorrelated PCs, samples could be mapped in a low dimensional space for discriminating [39,40]. The PC score plot of total 63 samples is shown in Fig. 9. Because PCA is an unsupervised method, the samples were clustered together only based on the similarities and differences in their PC scores. In PC1-PC2 space (Fig. 9a), each of 4 single odors occupied a separate region, and all binary mixtures were lying in new clusters. PC1 contained mainly information (88.78%) of original response matrix. Besides, for PC1, 4 single vapors were sorted by concentration in descending order. It indicated that the concentration information for vapors would be contained in PC1. In the PC1-PC3 space (Fig. 9b), most of samples were patterned in individual clusters. But an overlapped was observed in the samples from PA and PA + OA vapors. In addition, a well clustering result was observed in PC2-PC3 space (Fig. 9c) excepting a superposition between HA ($C_6$) and HPA ($C_7$) vapors. We can also find that for single vapor, the sort by PC2 is similar with that by molecular size. It might be contributed by the size effect of the imprinted template molecules. Besides, we can also find that the VOCs mixture samples were clustered on the centerline between two source VOCs in PC1-PC2 and PC1-PC3 spaces. However, in PC2-PC3 space, we did not find the similar result. It indicated that we could find a balance role in PCA spaces partly. The reason would be explained by the different concentrations for VOCs mixtures or pure organic acids.

To investigate the pattern recognition ability of MISG-LSPR multichannel sensor platform, LDA was applied in this study. Different from PCA, LDA is a supervised classifier by finding a discriminant function (DF), which is a linear combination of the original variables (features of the sensor responses) that tries to maximize the variance between groups and minimize the variance within groups [41,42]. More detail information about LDA can be found else here [43–46]. Here, the optimal transformation in LDA was achieved by minimizing the intragroup distances and maximizing the intergroup distances simultaneously, thus the best group discrimination could be obtained [47]. Similar to PCA, 2 discrimination functions were obtained by a linear combination of the 4 variables in the sensor array. Consequently, all samples could be plotted in a LDA space as shown in Fig. 10. It demonstrates the clear clustering of 7 distinct groups, which correspond to 4 single and 3 binary mixtures of organic acid vapors, with no overlap being observed. Taking into account a small number of samples in this study, full leave-one-out cross-validation (LOOCV) method was applied to validate LDA models in this study [48,49]. The LOOCV of LDA scores revealed a classification accuracy of 100%. It suggested that the multichannel LSPR-MISG sensor platform developed in this study could be applied on the pattern recognition of single or binary mixture of organic acid.

## 4. Conclusion

In summary, a MISG coated Au nano-island film was developed for determination of organic acids vapors selectively. The MISG reaction solution was spin coated on the Au nano-island layer. The results demonstrated that the adsorption capacity of pure $TiO_2$ sol-gel matrix was weak. In-situ response of HA-MISG was verified to be fast, selective and reversible. Eventually, by changing the template molecules in MISG reaction solutions, a 4 channels MISG-LSPR multichannel sensor array was constructed for the determination of 4 organic acids vapors (PA, HA, HPA and OA) in single and their binary mixtures. PCA and LDA were employed for pattern recognition of the response matrix. We also find a partly balance role between mixture VOCs and their source VOCs in PCA spaces. A 100% classification rate was achieved by leave-one-out cross-validation technique for the LDA model. It indicated that a sensor array combined MISG with LSPR could be an effective method for organic acid odor pattern recognition. This research offers some useful technologies for developing sensor system for organic acid from human body odor.

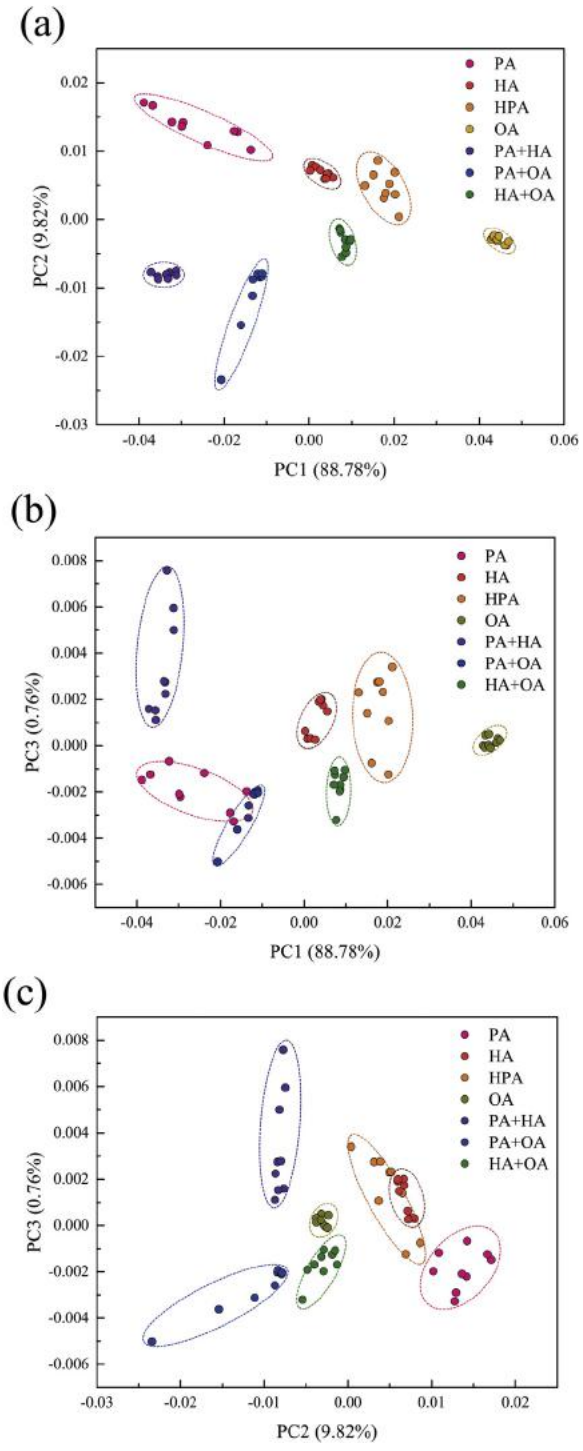


**Fig. 9.** PCA score plots of the multichannel responses for 63 samples from PA, HA, HPA, OA, binary mixture of PA + HA, PA + OA and HA + OA.

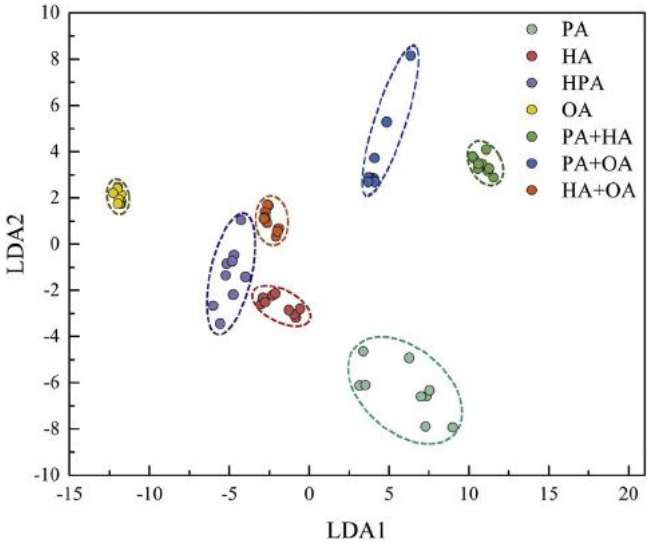


**Fig. 10.** LDA score plot of the first 2 discriminant factors (LDA1 and LDA2) achieved from transmittance change responses data of 63 samples from PA, HA, HPA, OA, binary mixture of PA + HA, PA + OA and HA + OA. Oval outlines indicate group of organic acid samples at 99% confidence level.

## Acknowledgments

This research was supported by a grant from China Scholarship Council (CSC), JSPS KAKENHI Grant Numbers (25420409, 15H01713) and the China Postdoctoral Science Foundation (No. 2016M602631).

## References

[1] M. Gallagher, J. Wysocki, J.J. Leyden, A.I. Spielman, X. Sun, G. Preti, Analyses of volatile organic compounds from human skin, Br. J. Dermatol. 159 (2008) 780–791.
[2] D.J. Penn, E. Oberzaucher, K. Grammer, G. Fischer, H.A. Soini, D. Wiesler, et al., Individual and gender fingerprints in human body odour, J. R. Soc. Interface 4 (2007) 331–340.
[3] S.K. Pandey, K.H. Kim, Human body-odor components and their determination, Trends Anal. Chem. 30 (2011) 784–796.
[4] M.L. Schaefer, D.A. Young, D. Restrepo, Olfactory fingerprints for major histocompatibility complex-determined body odors, J. Neurosci. 21 (2001) 2481–2487.
[5] M. Stitz, K. Gase, I.T. Baldwin, E. Gaquerel, Ectopic expression of atjmt in nicotiana attenuata: creating a metabolic sink has tissue-specific consequences for the jasmonate metabolic network and silences downstream gene expression, Plant Physiol. 157 (2011) 341–354.
[6] C.J. Liu, Y. Furusawa, K. Hayashi, Development of a fluorescent imaging sensor for the detection of human body sweat odor, Sens. Actuators B 183 (2013) 117–123.
[7] A.C. Little, B.C. Jones, R.P. Burriss, Preferences for masculinity in male bodies change across the menstrual cycle, Horm. Behav. 51 (2007) 633–639.
[8] R.J. Stevenson, An initial evaluation of the functions of human olfaction, Chem. Senses 35 (2010) 3–20.
[9] S.K. Jha, C.J. Liu, K. Hayashi, Molecular imprinted polyacrylic acids based qcm sensor array for recognition of organic acids in body odor, Sens. Actuators B 204 (2014) 74–87.
[10] S.K. Jha, K. Hayashi, Polyacrylic acid polymer and aldehydes template molecule based mips coated qcm sensors for detection of pattern aldehydes in body odor, Sens. Actuators B 206 (2015) 471–487.
[11] H. Ishida, Y. Wada, H. Matsukura, Chemical sensing in robotic applications: a review, IEEE Sens. J. 12 (2012) 3163–3173.
[12] D. Liu, M.Y. Liu, G.H. Liu, S.C. Zhang, Y.Y. Wu, X.R. Zhang, Dual-channel sensing of volatile organic compounds with semiconducting nanoparticles, Anal. Chem. 82 (2010) 66–68.
[13] A. Kaur, S. Ibrahim, C.J. Pickett, I.S. Michie, R.M. Dinsdale, A.J. Guwy, et al., Anode modification to improve the performance of a microbial fuel cell volatile fatty acid biosensor, Sens. Actuators B 201 (2014) 266–273.
[14] J. Kang, A.T. Hussain, M. Catt, M. Trenell, B. Haggett, E.H. Yu, Electrochemical detection of non-esterified fatty acid by layer-by-layer assembled enzyme electrodes, Sens. Actuators B 190 (2014) 535–541.
[15] A. Baliyan, P. Bhatia, B.D. Gupta, E.K. Sharma, A. Kumari, R. Gupta, Surface plasmon resonance based fiber optic sensor for the detection of triacylglycerides using gel entrapment technique, Sens. Actuators B 188 (2013) 917–922.
[16] B. Chen, C.J. Liu, M. Ota, K. Hayashi, Terpene detection based on localized surface plasma resonance of thiolate-modified au nanoparticles, IEEE Sens. J. 13 (2013) 1307–1314.
[17] B. Chen, C.J. Liu, M. Watanabe, K. Hayashi, Layer-by-layer structured aunp sensors for terpene vapor detection, IEEE Sens. J. 13 (2013) 4212–4219.
[18] H. Nanto, F. Yagi, H. Hasunuma, Y. Takei, S. Koyama, T. Oyabu, et al., Multichannel odor sensor utilizing surface plasmon resonance, Sens. Mater. 21 (2009) 201–208.

[19] K.M. Mayer, J.H. Hafner, Localized surface plasmon resonance sensors, Chem. Rev. 111 (2011) 3828–3857.
[20] J.B. Hu, Y. Yu, B. Jiao, S.Y. Ning, H. Dong, X. Hou, et al., Realizing improved performance of down-conversion white organic light-emitting diodes by localized surface plasmon resonance effect of ag nanoparticles, Org. Electron. 31 (2016) 234–239.
[21] M.J. Hou, Y. Huang, L.W. Ma, Z.J. Zhang, Sensitivity and reusability of sio2 nrs@ au nps sers substrate in trace monochlorobiphenyl detection, Nanoscale Res. Lett. 10 (2015).
[22] N.T. Li, D.M. Zhang, Q. Zhang, Y.L. Lu, J. Jiang, G.L. Liu, et al., Combining localized surface plasmon resonance with anodic stripping voltammetry for heavy metal ion detection, Sens. Actuators B 231 (2016) 349–356.
[23] B. Chen, M. Mokume, C.J. Liu, K. Hayashi, Structure and localized surface plasmon tuning of sputtered au nano-islands through thermal annealing, Vacuum 110 (2014) 94–101.
[24] A. Ersoz, S.E. Diltemiz, A.A. Ozcan, A. Denizli, R. Say, 8-ohdg sensing with mip based solid phase extraction and qcm technique, Sens. Actuators B 137 (2009) 7–11.
[25] H.N. Iqbal, P.A. Lieberzeit, Acidic and basic polymers for molecularly imprinted folic acid sensors-qcm studies with thin films and nanoparticles, Sens. Actuators B 176 (2013) 1090–1095.
[26] K. Kotova, M. Hussain, G. Mustafa, P.A. Lieberzeit, Mip sensors on the way to biotech applications: targeting selectivity, Sens. Actuators B 189 (2013) 199–202.
[27] U. Latif, A. Rohrer, P.A. Lieberzeit, F.L. Dickert, Qcm gas phase detection with ceramic materials-vocs and oil vapors, Anal. Bioanal. Chem. 400 (2011) 2457–2462.
[28] M. Matsuguchi, T. Uno, Molecular imprinting strategy for solvent molecules and its application for qcm-based voc vapor sensing, Sens. Actuators B 113 (2006) 94–99.
[29] Z.P. Yang, C.J. Zhang, Designing of mip-based qcm sensor for the determination of cu(II) ions in solution, Sens. Actuators B 142 (2009) 210–215.
[30] D.Z. Zhou, T.Y. Guo, Y. Yang, Z.P. Zhang, Surface imprinted macroporous film for high performance protein recognition in combination with quartz crystal microbalance, Sens. Actuators B 153 (2011) 96–102.
[31] R. Takemura, H. Sakata, H. Ishida, Active chemical sampling system for underwater chemical source localization, J. Sens. 2016 (2016) 11.
[32] F. Yoshino, T. Nakamoto, Odor recognition system using embedded leaning vector quantization circuit, Sensor Mater. 26 (2014) 137–147.
[33] B. Chen, M. Mokume, C.J. Liu, K. Hayashi, Irradiation wavelength-dependent photocurrent sensing characteristics of aunps/p3ht composites on volatile vapor, IEEE Sens. J. 16 (2016) 596–602.
[34] B. Chen, C.J. Liu, L.P. Ge, K. Hayashi, Localized surface plasmon resonance gas sensor of au nano-islands coated with molecularly imprinted polymer: influence of polymer thickness on sensitivity and selectivity, Sens. Actuators B 231 (2016) 787–792.
[35] B. Chen, C.J. Liu, K. Hayashi, Selective terpene vapor detection using molecularly imprinted polymer coated au nanoparticle lspr sensor, IEEE Sens. J. 14 (2014) 3458–3464.
[36] Y. Huang, X. Zhang, E. Ringe, M.J. Hou, L.W. Ma, Z.J. Zhang, Tunable lattice coupling of multipole plasmon modes and near-field enhancement in closely spaced gold nanorod arrays, Sci. Rep. 6 (2016).
[37] L. Shang, W.C. Guo, S.O. Nelson, Apple variety identification based on dielectric spectra and chemometric methods, Food Anal. Methods 8 (2015) 1042–1052.
[38] W.C. Guo, L. Shang, X.H. Zhu, S.O. Nelson, Nondestructive detection of soluble solids content of apples from dielectric spectra with ann and chemometric methods, Food Bioprocess Technol. 8 (2015) 1126–1138.
[39] L. Vera, L. Acena, J. Guasch, R. Boque, M. Mestres, O. Busto, Characterization and classification of the aroma of beer samples by means of an ms e-nose and chemometric tools, Anal. Bioanal. Chem. 399 (2011) 2073–2081.
[40] X.J. Zhang, L. You, E.V. Anslyn, X.H. Qian, Discrimination and classification of ginsenosides and ginsengs using bis-boronic acid receptors in dynamic multicomponent indicator displacement sensor arrays, Chem. Eur. J. 18 (2012) 1102–1110.
[41] A. Szczurek, M. Maciejewska, Recognition of benzene, toluene and xylene using tgs array integrated with linear and non-linear classifier, Talanta 64 (2004) 609–617.
[42] H. Kong, S.C. Zhang, N. Na, D. Liu, X.R. Zhang, Recognition of organic compounds in aqueous solutions by chemiluminescence on an array of catalytic nanoparticles, Analyst 134 (2009) 2441–2446.
[43] R. Kurita, H. Tabei, Z.M. Liu, T. Horiuchi, O. Niwa, Fabrication and electrochemical properties of an interdigitated array electrode in a microfabricated wall-jet cell, Sens. Actuators B 71 (2000) 82–89.
[44] J. Goschnick, I. Koronczi, M. Frietsch, I. Kiselev, Water pollution recognition with the electronic nose kamina, Sens. Actuators B 106 (2005) 182–186.
[45] A.H. Gomez, J. Wang, G.X. Hu, A.G. Pereira, Electronic nose technique potential monitoring mandarin maturity, Sens. Actuators B 113 (2006) 347–353.
[46] S. Panigrahi, S. Balasubramanian, H. Gu, C.M. Logue, M. Marchello, Design and development of a metal oxide based electronic nose for spoilage classification of beef, Sens. Actuators B 119 (2006) 2–14.
[47] R. Banerjee, B. Tudu, L. Shaw, A. Jana, N. Bhattacharyya, R. Bandyopadhyay, Instrumental testing of tea by combining the responses of electronic nose and tongue, J. Food Eng. 110 (2012) 356–363.
[48] J.M. Gutierrez, Z. Haddi, A. Amari, B. Bouchikhi, A. Mimendia, X. Ceto, et al., Hybrid electronic tongue based on multisensor data fusion for discrimination of beers, Sens. Actuators B 177 (2013) 989–996.
[49] J.P. Santos, M.J. Fernandez, J.L. Fontecha, J. Lozano, M. Aleixandre, M. Garcia, et al., Saw sensor array for wine discrimination, Sens. Actuators B 107 (2005) 291–295.

## Biographies

**Liang Shang** received the B.S. degree in mechanical manufacturing and automation and the M.S. degree in agricultural mechanization engineering from Northwest A&F University, Shannxi, China, in 2012 and 2015, respectively. He is currently pursuing the Ph.D. degree at Kyushu University, Fukuoka, Japan, and engaging in research related to gas and odor sensors.

**Chuanjun Liu** received his PhD degree in material engineering from Nagaoka University of Technology (Japan) in 2006. He has worked as research fellow in Nagaoka University of Technology (from 2006) and Kyushu University (from 2008), and as assistant professor at the Graduate School of Information Science and Electrical Engineering of Kyushu University (from 2012) and associate professor of R&D center for Taste and Odor Sensing (TAOS) of Kyushu University (from 2016). He is now a principle researcher in Research Laboratory of U.S.E. Co. LTD, Japan. He is a member of the Society of Polymer Science Japan and the Institute of Electrical Engineers of Japan. His research interests include the development and application of organic electronic devices, nanoscale sensing materials, and gas and odor sensors.

**Masashi Watanabe** received the B.S. and M.S. degree in engineering from Kyushu University, Fukuoka, Japan, in 2012 and 2014. He is currently pursuing the Ph.D. degree at the Graduate School of Information Science and Electrical Engineering, Kyushu University. His current research interests include nanostructures fabrication based on AuNPs and their application in chemical sensing devices.

**Bin Chen** received her PhD degree in the Graduate School of Information Science and Electrical Engineering from Kyushu University (Japan) in 2014. She is now a lecturer at the College of Electronic and Information Engineering at Southwest University, and engaging in the research of chemical sensors.

**Kenshi Hayashi** received his BE, ME, and PhD degree, all in electrical engineering, from Kyushu University (Japan) in 1982, 1984, and 1990, respectively. He is now a professor at the Graduate School of Information Science and Electrical Engineering of Kyushu University. He is a member of the Japan Society of Applied Physics and the Institute of Electrical Engineers of Japan. His research interests include: information service using odor cluster matching, visualization of odor space, measurement and coding of odor quality and quantity, novel devices using molecular wire and organic electronic material, and biometrics by odor sensing.